RSC Advances

PAPER

View Article Online
View Journal | View Issue



Cite this: *RSC Adv.*, 2017, **7**, 16704

# Reproducible and reliable resistive switching behaviors of $AlO_X/HfO_X$ bilayer structures with Al electrode by atomic layer deposition†

Masoud Akbari,‡ Min-Kyu Kim,‡ Dongshin Kim and Jang-Sik Lee*

Received 16th November 2016
Accepted 7th March 2017

DOI: 10.1039/c6ra26872b

rsc.li/rsc-advances

The resistive switching behaviors of $AlO_X/HfO_X$ bilayer structures were investigated. Metal oxides were deposited by atomic layer deposition. Al and Pt were used as top and bottom electrodes, respectively. Compared with $AlO_X$ and $HfO_X$ monolayer structures, the bilayer structure showed lower set/reset voltages and more-uniform resistive switching properties. It also exhibited good data retention and endurance. The Al top electrode may gather oxygen ions from the oxide layer underneath and thereby create oxygen vacancies in the oxide layer. The uniform electrical property of the bilayer structure is attributed to confined formation/rupture of conductive filaments in the $HfO_X$ layer, whereas undissociated filaments in the $AlO_X$ layer nucleate rapid regeneration of filaments.



## Introduction

Conventional charge-based memories are approaching their scaling limit, so alternative memory architectures are required. Resistive random access memory (RRAM) is one of the most promising candidates for next generation non-volatile memory devices due to its features, such as simple device structure, fast switching speed, and low power consumption.[1] Among various materials that have been studied, transition metal oxides such as $SrTiO_X$, $TiO_X$, $ZrO_X$, $AlO_X$, $HfO_X$, *etc.* have suitable performance in terms of resistive switching parameters.[2–8] In particular, RRAM based on these materials without active metal electrode have been called as valence change memory (VCM). Previous studies indicate that the resistive switching mechanism in VCM originates from migration of oxygen ions, whereby oxygen vacancies form a conductive filament under voltage sweep and consequently make the device switch from high-resistance state (HRS) to low-resistance state (LRS).[9,10]

Atomic layer deposition (ALD) is a thin film deposition technique that is widely used in semiconductor device fabrication.[11] ALD has unique characteristics, including a self-limiting deposition process, excellent conformality, atomic-scale thickness and composition control, and low-temperature deposition. ALD is typically used to deposit dielectric layers for MOSFETs and dynamic random access memory. These applications require a stoichiometric composition with ultra-low leakage current.[12]

An oxygen-deficient thin film is required for RRAM applications, so ALD process conditions need to be modified, or device structures need to be manipulated. To change the chemical composition of the film, some research groups have tried to change the ALD deposition conditions and recipes, *e.g.*, by altering the time duration of precursor exposure,[13] adjusting the mixture of oxidizer and inert gas,[14] conducting plasma treatment during deposition,[15] and changing substrate temperature.[13] However, modifying ALD conditions can cause deviation from the ALD window and degradation of properties of the film.[16]

As another approach, numerous studies have focused on manipulation of device structures by incorporating a chemically-active layer,[17,18] by doping,[19,20] and by using bilayer[5,21–23] and trilayer structures.[24] Due to fabrication simplicity to make bilayer RRAM, different structures have been studied, such as $ZrO_X/HfO_X$[21] and $WO_X/NbO_X$.[25] Inserting an Al layer between electrode and $HfO_X$ improves the switching uniformity, possibly by stabilizing the conductive filaments.[26] Moreover, $HfO_X/AlO_X$ bilayer stacks are capable of multilevel resistive switching.[27] In $TiN/HfO_2/Hf$ cells, embedding a thin $Al_2O_3$ at the $TiN/HfO_2$ or at the $Hf/HfO_2$ interface increases the memory window by increasing the concentration of defects.[28] Nevertheless, precise comparison of the resistive switching mechanism in such a bilayer device with those in monolayers remains necessary.

In this paper, we investigated resistive switching behavior of an $AlO_X/HfO_X$ bilayer structure deposited by ALD. The bilayer structure had uniform memory characteristics and good endurance properties; the uniform resistive switching behavior of bilayer structure emanates from partial dissociation of conductive filaments in the $HfO_X$ layer, whereas they remain stable in the $AlO_X$ layer during subsequent switching cycles.

*Department of Materials Science and Engineering, Pohang University of Science and Technology (POSTECH), Pohang 790-784, Republic of Korea. E-mail: jangsik@postech.ac.kr*

† Electronic supplementary information (ESI) available. See DOI: 10.1039/c6ra26872b

‡ These authors contributed equally to this work.

## Experimental

To fabricate the monolayer structures, a Ti adhesion layer (10 nm) was deposited on $SiO_2$/Si substrate using an electron beam evaporator. Then a Pt bottom electrode (100 nm) was deposited by sputtering. 5 nm $AlO_X$ or $HfO_X$ were deposited by ALD at 300 °C using trimethylaluminum (TMA) or tetrakis(ethylmethylamino)hafnium (TEMAHf) as precursors, respectively. For both oxides, $H_2O$ was used as the oxidizer and Ar as the purging gas. Finally, circular 100 nm-thick Al top electrodes with diameter of 50 μm were deposited on top of the oxide layer by e-beam evaporation through a metal shadow mask. In case of bilayer structures, after deposition of Ti adhesion layer and Pt bottom electrode, 3 nm $HfO_X$ was first deposited, followed by 3 nm $AlO_X$. The thickness of oxide was controlled by cycles of ALD and determined using spectroscopic ellipsometer (J.A. Woollam Co., M-2000_D). Then Al top electrodes were deposited on the oxide layers. The current–voltage (*I–V*) curve were measured using a Semiconductor Characterization System (KEITHLEY, 4200-SCS). The resistive switching speed and pulse response were measured using a waveform generator (33621A, KEYSIGHT) and oscilloscope (TDS 5054, TEKTRONIX). The response time of devices was tested by applying a single set or reset pulse to the device from a waveform generator. Then an *I–V* sweep with the semiconductor parameter analyzer was conducted to determine the device states. During electrical characterization the bottom electrode was grounded and voltage was applied to the top electrode. All measurements were performed at room temperature in ambient conditions, except the data retention measurement, which was performed at 85 °C. The X-ray photoelectron spectroscopy (XPS) depth profile of $AlO_X$/$HfO_X$ bilayer structure was analysed with X-ray photoelectron spectrometer (ESCA LAB250, VG SCIENTIFIC) using a monochromatic Al X-ray source (1486.6 eV) and Ar ion etching. The binding energies were calibrated by the C 1s peak at 284.8 eV. The crystal structure of $AlO_X$/$HfO_X$ bilayer was measured using X-ray diffraction (XRD, Rigaku D/MAX-2500) with Cu Kα radiation.

## Results and discussion

### Single $AlO_X$ device

Fig. 1 shows the resistive switching behaviors of Al/$AlO_X$/Pt device repeatedly measured for 50 cycles. The device was initially in HRS. To trigger resistive switching from HRS to LRS for the pristine devices, ~4 V electroforming voltage was needed. The device switched from HRS to LRS when positive voltage was applied, then returned to HRS during negative voltage sweeping; this behavior is known as bipolar resistive switching. Formation of conductive filaments under applied voltage bias is responsible for resistive switching in transition metal oxides.[9] Several studies have proven that top electrode element has an impact on memory performance.[17,29] The Al top electrode has high affinity for oxygen, and therefore functions as a reservoir of oxygen ions. Oxygen ions in the oxide layer migrate toward the top electrode interface under positive bias, and consequently leave oxygen vacancies in the oxide layer.

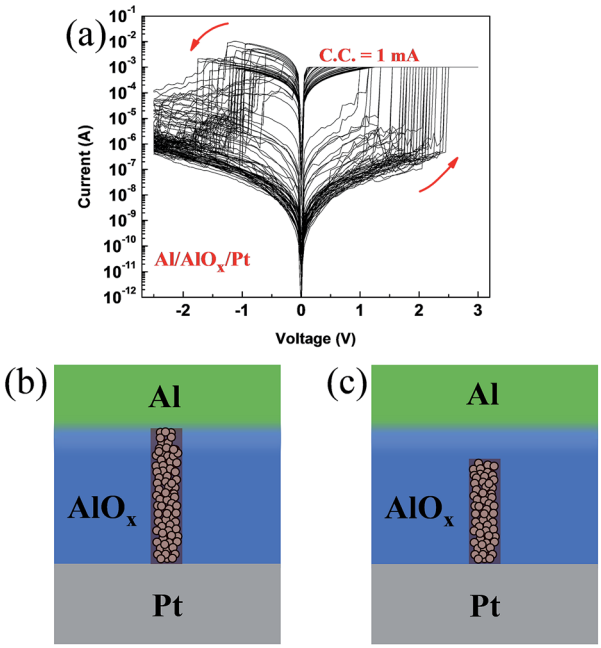


Fig. 1 (a) Typical *I–V* curves of RRAM devices with Al/$AlO_X$/Pt structure. Schematic representation of resistive switching mechanism for (b) low resistance state (LRS), and (c) high resistance state (HRS).

These vacancies form a conductive filament during the set process. When negative voltage is applied during the reset process, oxygen ions drift back into the oxide layer and recombine with vacancies; thus the filament dissociates and the device switches from LRS to HRS.[30]

According to the *I–V* curves (Fig. 1(a)), the device has a very sharp set and reset and also the ON/OFF ratio is relatively large. Moreover, current level at LRS is high. This behavior is similar to resistive switching behavior of conductive-bridge RAM (CBRAM) in which formation and rupture of a metallic filament causes sharp set/reset.[31] Bearing in mind that the device in our study is not a CBRAM, we can speculate that the above-mentioned behavior is due to formation/rupture of a very thick and dense filament made from oxygen vacancy (Fig. 1(b)). The $AlO_X$ layer might contain a large number of oxygen vacancies, which are created during deposition or through contact with Al top electrode. Under electric field, oxygen vacancies form a thick and dense filament, consequently, resistance significantly reduces and device switches to LRS. During negative bias dissociation of such a dense filament results in a sharp reset to HRS (Fig. 1(c)).

### Single $HfO_X$ device

In order to make a comparison, we changed the switching layer to $HfO_X$ deposited by ALD. Typical *I–V* curves of are shown in Fig. 2(a). Compared to $AlO_X$ device, electrical properties deteriorated. However, it is worthy of consideration that the repeating *I–V* curves fall into two main groups, one in which reset is sharp and resistance change is large (similar to *I–V* curves of $AlO_X$ device), and one in which reset is gradual and resistance change

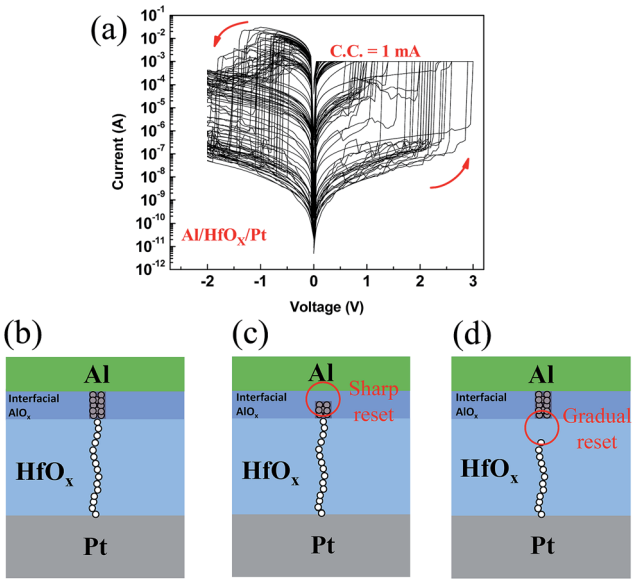


Fig. 2 (a) Typical *I*–*V* curves of RRAM devices with Al/HfO$_X$/Pt structure. Schematic representation of resistive switching mechanism for (b) LRS, (c) HRS with sharp reset, and (d) HRS with gradual reset.

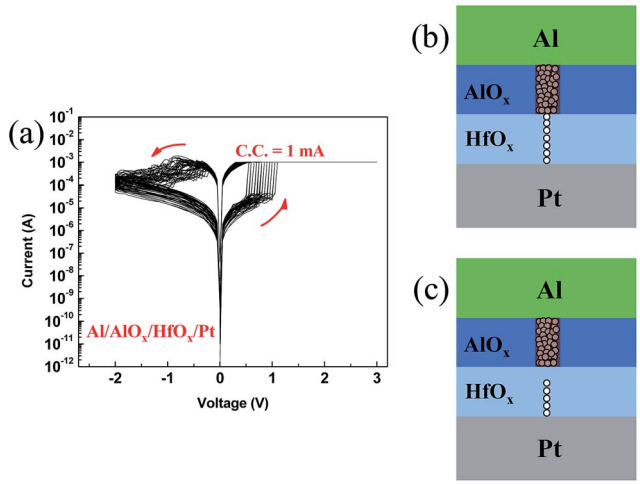


Fig. 3 (a) Typical *I*–*V* curves of RRAM devices with AlO$_X$/HfO$_X$ bilayer structure. Schematic representation of resistive switching mechanism for (b) LRS and (c) HRS, respectively.

is low. These diverse switching cycles occur quite randomly during repeating voltage sweep.

The presence of these two behaviors can be explained in terms of formation of a non-uniform filament. Since Al is chemically active, an interfacial AlO$_X$ layer is formed between electrode and HfO$_X$ layer.[30,32] Accordingly, we can consider the device structure as a bilayer AlO$_X$/HfO$_X$ that the formed filament in each layer might be dissimilar (Fig. 2(b)). By comparing the *I*–*V* characteristics of AlO$_X$ and HfO$_X$, we suggest that filament in interfacial AlO$_X$ layer might be larger than the one in HfO$_X$ layer; therefore, during reset process if the thick filament in interfacial AlO$_X$ is dissociated, resistance sharply reduces and device goes to very low resistance state (Fig. 2(c)). Likewise, if the weak filament in HfO$_X$ layer is ruptured, reset is gradual and resistance change is lower (Fig. 2(d)).

### Bilayer AlO$_X$/HfO$_X$ device

The randomness of the observed different switching in HfO$_X$ device can be due to instability of filament in both oxides. Considering the thick and dense filament in AlO$_X$ device on the one hand, and two different HRS levels in HfO$_X$ device on the other hand, we intentionally deposited bilayer AlO$_X$/HfO$_X$ device by ALD. The bilayer structure of AlO$_X$/HfO$_X$/Pt was confirmed by XPS depth profile (Fig. S1(a)†). When devices were fabricated with AlO$_X$/HfO$_X$ bilayer structure, 3 nm of each layer was chosen for lower operation voltages as well as reliable operation. The crystal structure of AlO$_X$/HfO$_X$ layer was measured by XRD. As shown in Fig. S1(b),† there is only Pt (111) peak and any peaks of AlO$_X$/HfO$_X$ layer were not found. This result may indicate that AlO$_X$/HfO$_X$ bilayer is amorphous, but further study using high resolution electron microscopy needs to be done to clarify the crystallization nature. Typical *I*–*V* curves are shown in Fig. 3(a). Interestingly, bilayer device shows uniform resistive switching during repeated cycles and low set/reset voltages with a gradual reset process. The schematic representation of resistive switching mechanism in the bilayer AlO$_X$/HfO$_X$ device is shown in Fig. 3(b and c). Filament that forms in AlO$_X$ layer is proportionately thick and stable while in HfO$_X$ layer is weak (Fig. 3(b)), so during the reset process only the weak filaments in the HfO$_X$ layer dissociate (Fig. 3(c)). The undissociated filaments in the AlO$_X$ layer nucleate regrowth of filaments during the next set process.[33] This process reduces the randomness of formation of filament and consequently improves the uniformity of resistive switching in the bilayer structure. Analogous to this mechanism, some studies have suggested partial formation/rupture of filaments in other bilayer RRAM devices.[25,34] Fig. 4(a) shows distribution of set voltages of devices. The bilayer device showed more uniform resistive switching during repeated cycles than the monolayer devices. The AlO$_X$/HfO$_X$ bilayer structure had significantly more uniform resistance of LRS/HRS than the monolayer devices (Fig. 4(b)). In practical application, broad distribution of RRAM parameters such as operation voltages and resistance in HRS and LRS has been issues.[35] In this view, this method to improve the uniformity of RRAM devices can be a good solution.

In order to verify controllability of filament further, we applied different negative voltage in reset process (Fig. 5(a)). Due to the gradual reset process in the AlO$_X$/HfO$_X$ bilayer

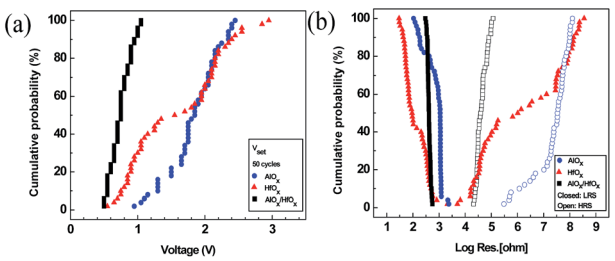


Fig. 4 Cycle-to-cycle cumulative probability distribution of (a) set/reset voltages and (b) LRS/HRS resistance states.

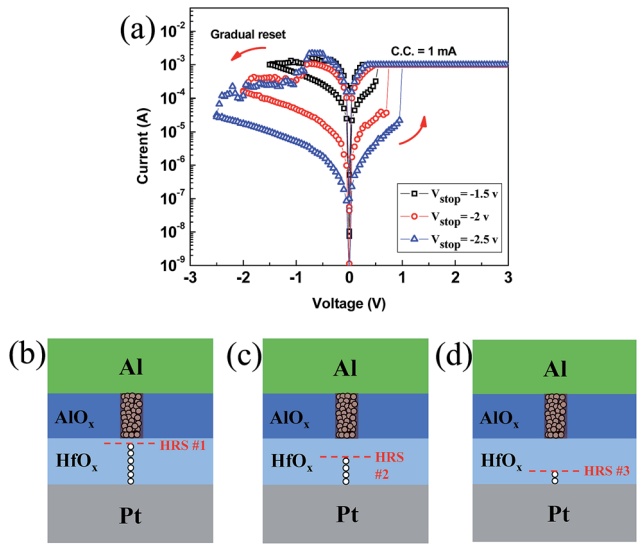


Fig. 5 (a) Typical *I*–*V* curves of $AlO_X/HfO_X$ bilayer structure measured at different reset stop voltages to show controllability of filament. (b–d) Schematic representation of resistive switching mechanism for 3 different HRS #1–3, respectively.

structure, selecting different stop points (−1.5, −2 and −2.5 V) will lead to create diverse HRS levels (HRS 1–3#). The magnitude of HRS level depends on the proportion of filament that dissociates under negative electric field (Fig. 5(b–d)). When reset stop point is small (−1 V) a slight amount of filament in $HfO_X$ layer dissolves and consequently resistance change will be low. The higher negative voltage is applied, the lower HRS level will be achieved. Besides, filament in $AlO_X$ layer remains stable. This indicates that such a bilayer structure brings about controllability of filament, as well as the ability to modify resistive switching behavior. Good endurance properties and data retention are essential in non-volatile memory applications. To estimate the electrical reliability of our devices, endurance properties and data retention were measured. In endurance test, set voltage pulse (+4 V, 10 ms) and reset voltage pulse (−3 V, 10 ms) were used (Fig. S2†). The bilayer structure showed some fluctuations in HRS during endurance cycles, but resistive switching maintained stable for more than 400 cycles, whereas $AlO_X$ and $HfO_X$ devices failed after around 170 and 220 cycles, respectively (Fig. 6(a)). Data retention tests of the bilayer structure were conducted at 85 °C. The device remained stable without any noticeable degradation (Fig. 6(b)). Similar data retention property was also observed at room temperature. Further improvement of endurance and data retention properties is being done based on this study by the optimization of various process conditions and device dimension scaling.

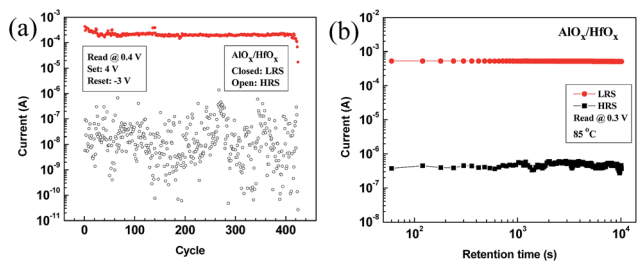


Fig. 6 (a) Pulse endurance test of $AlO_X/HfO_X$ bilayer structures. (b) Data retention characteristics of $AlO_X/HfO_X$ bilayer structure at 85 °C.

We measured switching speed of RRAM device with $AlO_X/HfO_X$ bilayer structure. When we applied 100 ns pulse with amplitude of 2 V, the state of devices was changed from HRS to LRS. The state of devices was confirmed by dc voltage sweep before and after applying bias pulses (Fig. S3(a)†). In the same way, reset process is confirmed by applying 100 ns pulse with amplitude of −3 V (Fig. S3(b)†). The 100 ns pulse width was enough to switch the resistance state of devices. In addition resistive switching behavior in pulse mode verified by set–read–reset–read pulse cycle tests (Fig. S3(c)†).

## Conclusions

In conclusion, we investigated the resistive switching behaviors of $AlO_X/HfO_X$ bilayer structures. By using Al as the top electrode and $AlO_X/HfO_X$ bilayer structures, memory devices had reproducible and reliable resistive switching operations, good endurance, and good data retention properties. We suggest that the uniform and reliable switching behaviors may be due to confined formation and dissociation of filaments in the bilayer structures; *i.e.* filaments in $HfO_X$ layer are weak and they form/dissociate during set/reset, while filaments in $AlO_X$ layer are thick, and they remain stable during set/reset. The undissociated filaments in the $AlO_X$ layer facilitate the nucleation and regrowth of filament in $HfO_X$ layer. This study provides an easy ALD process to fabricate reliable resistive switching memory devices with simple device structures for potential application to future nonvolatile memory industry.

## Acknowledgements

This work was supported by National Research Foundation of Korea (NRF-2016M3D1A1027663, NRF-2015R1A2A1A15055918). This work was also supported by Future Semiconductor Device Technology Development Program (10045226) funded by the Ministry of Trade, Industry & Energy (MOTIE)/Korea Semiconductor Research Consortium (KSRC). In addition, this work was partially supported by Brain Korea 21 PLUS project (Center for Creative Industrial Materials).

## Notes and references

1 R. Waser, R. Dittmann, G. Staikov and K. Szot, *Adv. Mater.*, 2009, **21**, 2632–2663.
2 H.-S. Wong, H.-Y. Lee, S. Yu, Y.-S. Chen, Y. Wu, P.-S. Chen, B. Lee, F. T. Chen and M.-J. Tsai, *Proc. IEEE*, 2012, **100**, 1951–1970.
3 Y. Huang, Z. H. Shen, Y. Wu, X. Q. Wang, S. F. Zhang, X. Q. Shi and H. B. Zeng, *RSC Adv.*, 2016, **6**, 17867–17872.
4 Y. Huang, Z. H. Shen, Y. Wu, M. Q. Xie, Y. Q. Hu, S. F. Zhang, X. Q. Shi and H. B. Zeng, *AIP. Adv.*, 2016, **6**, 025018.

5 M.-K. Kim and J.-S. Lee, *ACS Appl. Mater. Interfaces*, 2016, **8**, 32918–32924.
6 K. Park and J.-S. Lee, *Nanotechnology*, 2016, **27**, 125203.
7 U. B. Han and J. S. Lee, *Sci. Rep.*, 2016, **6**, 25537.
8 U. B. Han and J. S. Lee, *Sci. Rep.*, 2016, **6**, 28966.
9 C.-Y. Lin, C.-Y. Wu, C.-Y. Wu, C. Hu and T.-Y. Tseng, *J. Electrochem. Soc.*, 2007, **154**, G189–G192.
10 S. Long, X. Lian, C. Cagli, X. Cartoixa, R. Rurali, E. Miranda, D. Jiménez, L. Perniola, M. Liu and J. Suñé, *Appl. Phys. Lett.*, 2013, **102**, 183505.
11 H. Kim, H.-B.-R. Lee and W.-J. Maeng, *Thin Solid Films*, 2009, **517**, 2563–2580.
12 S. M. George, *Chem. Rev.*, 2009, **110**, 111–131.
13 J. J. Yang, N. P. Kobayashi, J. P. Strachan, M.-X. Zhang, D. A. Ohlberg, M. D. Pickett, Z. Li, G. Medeiros-Ribeiro and R. S. Williams, *Chem. Mater.*, 2010, **23**, 123–125.
14 S.-J. Park, J.-P. Lee, J. S. Jang, H. Rhu, H. Yu, B. Y. You, C. S. Kim, K. J. Kim, Y. J. Cho and S. Baik, *Nanotechnology*, 2013, **24**, 295202.
15 T.-H. Jung, J.-S. Park, D.-H. Kim, Y. Jeong, S.-G. Park and J.-D. Kwon, *J. Vac. Sci. Technol., A*, 2013, **31**, 01A124.
16 R. A. Fischer, *Precursor chemistry of advanced materials: CVD, ALD and nanoparticles*, Springer, 2005.
17 H. Y. Jeong, J. Y. Lee and S. Y. Choi, *Adv. Funct. Mater.*, 2010, **20**, 3912–3917.
18 Y. Wu, B. Lee and H.-S. Philip Wong, *IEEE Electron Device Lett.*, 2010, **31**, 1449–1451.
19 C.-S. Peng, W.-Y. Chang, Y.-H. Lee, M.-H. Lin, F. Chen and M.-J. Tsai, *Electrochem. Solid-State Lett.*, 2012, **15**, H88–H90.
20 M. Akbari and J. S. Lee, *RSC Adv.*, 2016, **6**, 21917–21921.
21 J. Lee, E. M. Bourim, W. Lee, J. Park, M. Jo, S. Jung, J. Shin and H. Hwang, *Appl. Phys. Lett.*, 2010, **97**, 172105.
22 J.-K. Lee, S. Jung, J. Park, S.-W. Chung, J. S. Roh, S.-J. Hong, I. H. Cho, H.-I. Kwon, C. H. Park and B.-G. Park, *Appl. Phys. Lett.*, 2012, **101**, 103506.
23 K. Park and J. S. Lee, *RSC Adv.*, 2016, **6**, 21736–21741.
24 L. G. Wang, X. Qian, Y. Q. Cao, Z. Y. Cao, G. Y. Fang, A. D. Li and D. Wu, *Nanoscale Res. Lett.*, 2015, **10**, 1–8.
25 S. M. Sadaf, X. Liu, M. Son, S. Park, S. H. Choudhury, E. Cha, M. Siddik, J. Shin and H. Hwang, *Phys. Status Solidi A*, 2012, **209**, 1179–1183.
26 S. Yu, B. Gao, H. Dai, B. Sun, L. Liu, X. Liu, R. Han, J. Kang and B. Yu, *Electrochem. Solid-State Lett.*, 2010, **13**, H36–H38.
27 S. Yu, Y. Wu and H.-S. P. Wong, *Appl. Phys. Lett.*, 2011, **98**, 103514.
28 L. Goux, A. Fantini, B. Govoreanu, G. Kar, S. Clima, Y.-Y. Chen, R. Degraeve, D. Wouters, G. Pourtois and M. Jurczak, *Electrochem. Solid-State Lett.*, 2012, **1**, P63–P65.
29 H. Y. Jeong, S. K. Kim, J. Y. Lee and S.-Y. Choi, *J. Electrochem. Soc.*, 2011, **158**, H979–H982.
30 C. Chen, S. Gao, F. Zeng, G. Tang, S. Li, C. Song, H. Fu and F. Pan, *J. Appl. Phys.*, 2013, **114**, 014502.
31 I. Valov, R. Waser, J. R. Jameson and M. N. Kozicki, *Nanotechnology*, 2011, **22**, 254003.
32 M. Hota, C. Mukherjee, T. Das and C. Maiti, *ECS J. Solid State Sci. Technol.*, 2012, **1**, N149–N152.
33 S. Yu, Y. Wu, Y. Chai, J. Provine and H.-S. Wong, *Presented in part at the Symposium on VLSI Technology, Systems and Applications (VLSI-TSA)*, Hsinchu, 25–27 April 2011.
34 H. Lv, H. Wan and T. Tang, *IEEE Electron Device Lett.*, 2010, **31**, 978–980.
35 S. W. Ryu, S. Cho, J. Park, J. Kwac, H. J. Kim and Y. Nishi, *Appl. Phys. Lett.*, 2014, **105**, 072102.